Spin Excitations in a $4f-3d$ Heterodimer on MgO

A. Singha,[1,2,3] F. Donati,[1,2,3] F. D. Natterer,[2,4] C. Wäckerlin,[2,5] S. Stavrić,[6] Z. S. Popović,[6] Ž. Šljivančanin,[6,7] F. Patthey,[2] and H. Brune[2]

[1]*Center for Quantum Nanoscience, Institute for Basic Science (IBS), Seoul 03760, Republic of Korea*
[2]*Institute of Physics, École Polytechnique Fédérale de Lausanne, Station 3, CH-1015 Lausanne, Switzerland*
[3]*Department of Physics, Ewha Womans University, Seoul 03760, Republic of Korea*
[4]*Physik-Institut, Universität Zürich, Winterthurerstrasse 190, CH-8057 Zürich, Switzerland*
[5]*Nanoscale Materials Science, Empa, Swiss Federal Laboratories for Materials Science and Technology, 8600 Dübendorf, Switzerland*
[6]*Vinča Institute of Nuclear Sciences, University of Belgrade, P.O. Box 522, RS-11001 Belgrade, Serbia*
[7]*Texas A&M University at Qatar, P.O. Box 23874, Education City, Doha, Qatar*

(Received 8 July 2018; revised manuscript received 18 October 2018; published 18 December 2018)

We report on the magnetic properties of HoCo dimers as a model system for the smallest intermetallic compound of a lanthanide and a transition metal atom. The dimers are adsorbed on ultrathin MgO(100) films grown on Ag(100). New for $4f$ elements, we detect inelastic excitations with scanning tunneling spectroscopy and prove their magnetic origin by applying an external magnetic field. In combination with density functional theory and spin Hamiltonian analysis, we determine the magnetic level distribution, as well as sign and magnitude of the exchange interaction between the two atoms. In contrast to typical $4f-3d$ bulk compounds, we find ferromagnetic coupling in the dimer.

DOI: 10.1103/PhysRevLett.121.257202

Many alloys combining transition metal (TM) elements of the first row with rare earth (RE) elements are widely used as permanent magnets due to their large magnetic anisotropy and remanent magnetization. The coupling between the spins of these elements can give rise to complex magnetic structures that exhibit rich phase diagrams [1]. This is due to the indirect exchange interaction between the $4f$ orbitals of the RE and the $3d$ orbitals of the TM mediated by the spd conduction electrons [2]. In addition, the magnetic order of RE-TM alloys is strongly affected by structural relaxations and surface effects [3]. Both become particularly important when the size of the magnet reaches atomic dimensions [4–8].

Understanding the magnetic level distribution and, therefore, the origin of magnetic anisotropy is important for the rational design of prototypical nanomagnets. The splitting of the low energy levels can be investigated using scanning tunneling microscopy (STM) and spin-excitation spectroscopy (SES) [9]. However, the detection of spin-excitations in $4f$ atoms and $4f$ single molecule magnets is very challenging due to the vanishing contribution of the $4f$ electrons to the tunnel current as a result of their strong localization [10,11], and reading the magnetic state of adsorbed RE atoms and islands is possibly enabled by the exchange interaction with the $5d$ shell [10,12]. Accordingly, spin-excitations have not been reported in $4f$ containing nanostructures, including single molecule magnets, apart from claims that, however, were not substantiated by demonstrating their Zeeman shifts [13–15]. Also, for some of the claimed systems [14], the inelastic features and associated magnetic properties could not be reproduced [11,16]. In contrast to the strongly localized $4f$ electrons, the $3d$ orbitals of TM atoms are more directly probed by tunneling electrons, and therefore, they often exhibit large SES cross sections [17]. In order to access the magnetism of $4f$ elements via SES, we combine one RE atom with one TM atom and study the magnetism of this heterodimer, which is also a model system for probing the $4f-3d$ exchange coupling at the atomic scale.

We report on the magnetic properties of HoCo heterodimers on MgO(100) thin films grown on Ag(100) [18]. The properties of Ho and Co on MgO are particularly intriguing: Ho on MgO is the first discovered single atom magnet which exhibits a magnetic moment that is close to its highest possible value [33–35], whereas Co on the same surface exhibits the largest magnetic anisotropy energy [17]. The MgO(100) thin films grown on metal surfaces are ideal substrates as MgO decouples the magnetic states of adsorbates from the scattering of substrate electrons and soft phonons [33,36]. For HoCo dimers, we observe two pairs of spin-excitations at ± 8 and ± 20 meV, for which we develop an effective spin Hamiltonian (SH) [18] using minimal input from our density functional theory (DFT) calculations [18]. The SH model reproduces the magnetic field dependent conductance steps. In agreement with DFT, this model finds collinear ferromagnetic coupling between Ho and Co. The DFT inferred adsorption site is also in agreement with experiment. Using SH, we determine the

magnetic level spectrum of HoCo and the relative contribution of the two elements to the experimentally detected spin excitations.

The Ho and Co atoms were codeposited onto the cold substrates, in the measurement position of our 0.4 K, ±8 T home-built STM [37]. This yields predominantly individual Ho and Co atoms, but also the occasional formation of homodimers and heterodimers. In order to unequivocally distinguish the different species, we prepared samples separately with only Ho or only Co. Each species has characteristic inelastic conductance (dI/dV) steps and/or apparent heights. The homodimers, Ho_2 and Co_2, show intense dI/dV steps located at ±85 and ±13 meV, respectively (Figs. S1 and S2 [18]). Figure 1(a) shows an STM image of the remaining four species. Isolated Ho atoms adsorb on top of O (Ho^{top}) or bridge sites (Ho^{br}) of the MgO(100) lattice [38]. They are discerned by their distinct apparent heights [Fig. 1(b)]; neither one has observable inelastic conductance steps [Fig. 1(e)]. Isolated Co atoms adsorb on top of O only [38] and are clearly identified by their dI/dV steps at ±58 meV, reminiscent of their high magnetic anisotropy [17]. The apparent height of the HoCo dimer is distinct from Ho^{br}, Ho^{top}, and Co atoms [Fig. 1(b)], and it possesses an "egglike" footprint with its axis aligned along the MgO (100) lattice directions [Fig. 1(c)]. This shape, as well as the location of the dimer, are in agreement with the adsorption geometry inferred from DFT, where Ho and Co adsorb on two adjacent O sites with vertical distances of 2.26 and 1.89 Å [Fig. 1(d)].

The spectroscopic fingerprints of the heterodimer are conductance steps at ±20 meV [Fig. 1(e)]. Their magnetic origin becomes evident from their linear shift in an out-of-plane external magnetic field [Fig. 2(a)]. This spin excitation is markedly different than the behavior of individual Ho and Co atoms on the same substrate, unlike the case of Fe-Ho pairs adsorbed on Pt(111), where the spin excitation of the Fe atom remains unchanged upon approaching the Ho atom to 4.24 Å distance [11]. Figure 2(b) displays the magnetic field and MgO thickness-dependent excitation energies for several HoCo dimers. From a linear fit to the step energy $E(H) = g\mu_0 H \Delta m \mu_B$ [Fig. 2(b)], we extract the effective Landé g factor of 3.1 ± 0.3 assuming $\Delta m = \pm 1$ (Tables I and II of Supplemental Material [18]), where Δm is the change in the out-of-plane component of the total magnetic moment. The large mean value of g indicates the presence of a sizable orbital moment, consistent with a previous report for Fe atoms on MgO [39].

As can be seen from Fig. 2(b), the step energy depends strongly on MgO thickness (i.e., it moves to lower energy by 1.7 meV on thicker MgO layers) and, also, weakly on the local environment of a given dimer (variance of 0.2 meV for the dimer shown with gray triangles). According to DFT, the adsorption of the HoCo dimers leads to sizeable distortions of the underlying MgO lattice. These distortions as well as the crystal fields for 1 and 2 ML MgO/Ag(100) are different. This leads to the lower excitation energies observed for HoCo dimers adsorbed on thicker MgO films. Similar thickness dependent behavior was also observed for Fe atoms on MgO [40].

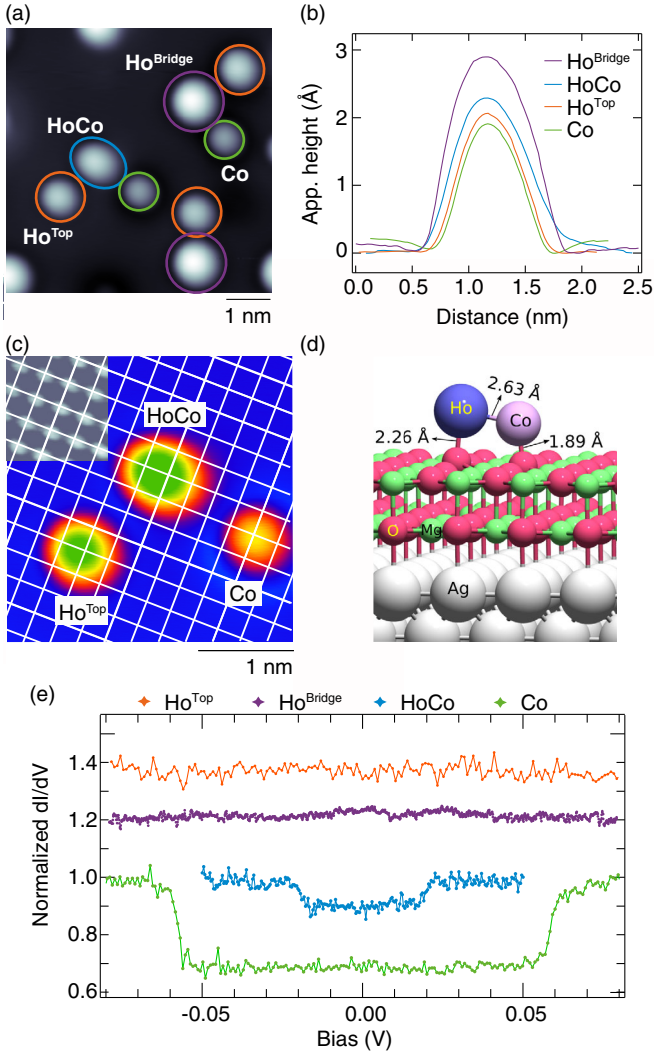

FIG. 1. Identification of HoCo dimers and detection of their spin excitations. (a) STM image and (b) apparent height profiles of HoCo dimer and individual Ho^{top}, Ho^{br}, and Co atoms. (c) STM image showing the characteristic elliptical shape of a HoCo dimer in comparison with the more symmetric shape of individual Ho and Co atoms [(a)–(c) $V_t = 100$ mV, $I_t = 50$ pA, and $\mu_0 H = 6$ T, $T = 4.3$ K]. Inset: atomic resolution image of 2 ML MgO with O imaged bright ($V_t = 10$ mV, $I_t = 8$ nA). The white grid shows the O sublattice [38]. (d) DFT calculated adsorption geometry of HoCo. (e) dI/dV of HoCo dimer ($V_t = 40$ mV, $I_t = 250$ pA), Ho^{top}, Ho^{br}, and Co atoms ($V_t = 100$ mV, $I_t = 500$ pA). All spectra: $V_{mod,ptp} = 1$ mV, $\mu_0 H = 1$ T, $T = 4.3$ K. For clarity, Ho^{top} and Ho^{br} spectra are vertically offset by 0.2 each.

We expect two types of magnetic excitations in dimers, one where the total magnetic moment $\hat{\mathbf{S}}$ changes and one where its projection $\hat{S}_z$ does [41]. The fact that only one

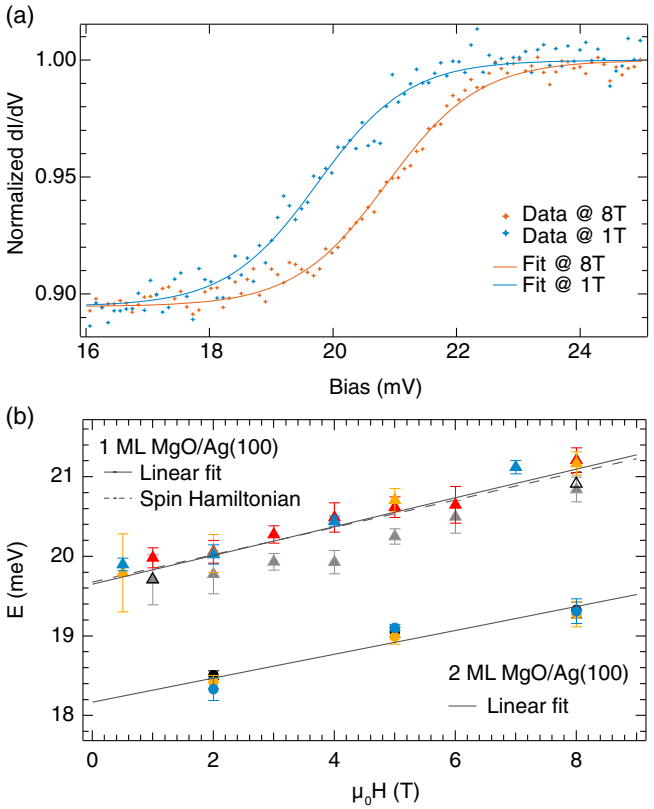

FIG. 2. (a) Magnetic field dependence of the dI/dV step of a HoCo dimer (dots: raw data; lines: sigmoid fits). Each data point represents the average from 10 spectra recorded on the same HoCo dimer ($V_t = 30$ mV, $I_t = 750$ pA, $V_{mod,ptp} = 500$ μV, $T = 0.4$ K). (b) Zeeman plot obtained from measurements on four HoCo dimers adsorbed on 1 ML MgO/Ag(100) (filled triangles) and three HoCo dimers on 2 ML MgO/Ag(100) (filled circles) ($T = 4$ K). Different colors represent the individual heterodimers. The 0.4 K measurements shown in (a) are included as open black triangles. Error bars represent the standard deviation from ≥ 5 measurements on the same heterodimer. The dashed line shows a fit with the spin Hamiltonian described in the text ($D = -0.47$ meV, $J = -1.43$ meV, $g_{Co} = 3.2$).

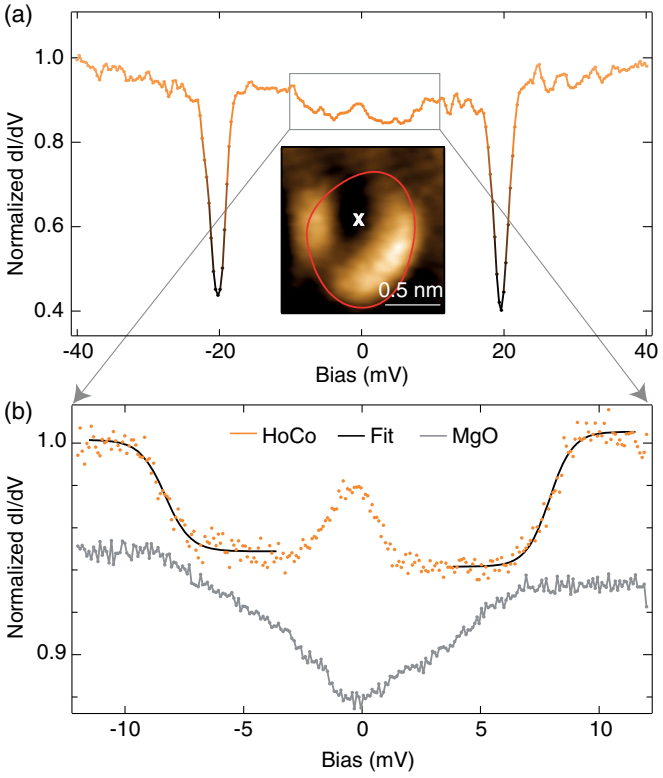

FIG. 3. (a) dI/dV spectra measured with a spin-polarized tip at the center of a HoCo dimer (dots: measurements, lines: sigmoid fits). Inset shows the corresponding dI/dV map measured at $V_t = 20$ mV overlaid with the contour of 15% of the maximum apparent height of the heterodimer. In addition to the jagged inelastic features at ± 20 meV, a pair of inner steps are detected at about ± 8.1 meV ($V_t = 40$ mV, $I_t = 1$ nA, and $V_{mod,ptp} = 500$ μV). (b) Zoom on the inner step shown in (a). Each data point represents the average from five acquisitions. ($V_t = 15$ mV, $I_t = 300$ pA, and $V_{mod,ptp} = 200$ μV). $\mu_0 H = 8$ T and $T = 0.4$ K for both figures.

transition is observed suggests that the intensity of the second is below our detection limit. Therefore, we used spin-polarized (SP) STM tips that can enhance the cross section of spin-excitation processes allowing us to probe very weak SES transitions [39,42]. We spin polarized the current by transferring Co atoms to the tip until a signature of spin polarization in the SES of Co is observed (Fig. S3 [18]) [39]. Figure 3(a) shows that the steps at ± 20 meV are now intense dips, indicative of spin pumping [43], and indeed, an additional pair of symmetric steps at ± 8.1 meV become apparent [Fig. 3(b)]. Being only 13% of the ± 20 meV step conductance, this transition would have a conductance variation of merely 1% without SP, and thus, it is obscured by noise in Fig. 1(e). Note that the zero-bias dip in the dI/dV spectra measured on the surface and the concomitant peak in the corresponding measurement on the dimer may stem from different quantum interference paths of the tunneling electrons in the presence of the SP tip. A similar zero-bias peak has also been observed for Fe atoms on MgO with an SP tip [39].

The observed inelastic features are mapped onto an effective spin Hamiltonian (SH) of the following form: $\hat{H} = D\hat{S}_z^2 + J(\hat{\mathbf{S}}_{Ho} \cdot \hat{\mathbf{S}}_{Co}) + \mu_B[g_{Ho}\hat{\mathbf{S}}_{Ho} + g_{Co}\hat{\mathbf{S}}_{Co}] \cdot \mu_0 \mathbf{H}$, where D is the uniaxial out-of-plane (z-axis) anisotropy, J is the Heisenberg exchange coupling between effective Ho and Co spin, and the last term is the Zeeman energy due to the external field acting on both effective spins.

The effective spin values define the level multiplicity of the lowest multiplet. For RE elements the spin-orbit coupling largely dominates over the crystal field and, therefore, the effective spin can be well described using the total magnetic moment (orbital + spin) [44]. Accordingly, for Ho, we consider the $4f$ occupancy obtained from DFT calculations of 11.02, and deduce the total magnetic moment as the highest possible projection in the $4f^{11}$

configuration. This yields $g_{\mathrm{Ho}} = 1.2$ and $S_{\mathrm{Ho}} = 15/2$. In contrast, for TMs the hierarchy of interactions is reversed. Consequently, the total moment is no longer a good quantum number [17,39]. In particular, for low symmetry environments, the level multiplicity can be defined by the spin moment only [45,46]. Therefore, for Co, we take the spin magnetic moment $S_{\mathrm{Co}} = 1$ calculated from DFT, and include the possibility of a nonvanishing orbital component through g_{Co}. This leaves D, J, and g_{Co} as the only free parameters. Note that the Ho-4f and Co-3d occupancy in the dimer differ from the respective single atom counterparts [17,33].

Both inelastic steps, as well as the large effective g factor for the spin excitation at ± 20 meV, are reproduced with $D = -0.46 \pm 0.02$ meV (out-of-plane easy axis), $J = -1.42 \pm 0.05$ meV (ferromagnetic coupling), and $g_{\mathrm{Co}} = 3.2 \pm 0.1$. Figure 2(b) illustrates the excellent agreement between the measured (full line) and calculated (dashed line) Zeeman shift of the step energy. A positive J would yield $g < 2$, which contradicts our experimental observation of $g = 3.1 \pm 0.3$. The ferromagnetic coupling between the two atoms in the heterodimer is also found in DFT, in contrast to the ferrimagnetic exchange reported for most bulk RE-TM alloys [47]. Note that applying an out-of-plane magnetic field leads to a significantly higher g factor compared to a free electron value of 2. This suggests an out-of-plane easy axis of the heterodimer, in contrast to the in-plane orientation calculated from DFT.

Figure 4 sketches the ground state and the first two excited states which are accessible in the presence of the $\Delta S = \pm 1, 0$ selection rules [45]. The two observed transitions are $|S, S_z\rangle = |17/2, \pm 17/2\rangle \rightarrow |15/2, \pm 15/2\rangle$, for which we calculate 21.1 meV at 8 T, and $|17/2, \pm 17/2\rangle \rightarrow |17/2, \pm 15/2\rangle$, for which our SH yields 8.2 meV at 8 T.

In order to quantify the contribution of each atom to S_z, we compute the expectation value of $S_{z,\mathrm{Ho}}$ and $S_{z,\mathrm{Co}}$ (Supplemental Material [18]) and show them on the right-hand side of Fig. 4. The prominent inelastic transition observed at ± 20 meV is dominated by an almost 90% reduction of $S_{z,\mathrm{Co}}$, whereas the out-of-plane projection of the Ho moment is reduced only by a few percent. If we assumed that the tunnel electrons interacted mostly with the TM element, this would explain the larger step height for this transition implying a strong change of $S_{z,\mathrm{Co}}$. For the inner steps at ± 8.1 meV the opposite is true; i.e., the change of the out-of-plane projected overall magnetic moment of the dimer is mostly due to the Ho atom, again in agreement with the observation of these steps having low intensity. Finally, we attribute the large $g_{\mathrm{Co}} = 3.2$ value to an unquenched orbital moment contribution of $m_L = 1.2\mu_{\mathrm{B}}$ [18]. This value compares well with previous reports for single surface-supported Co atoms [48,49]. However, it is strongly reduced compared to the maximum orbital moment of Co atoms on MgO [17], due to the lowered symmetry caused by the neighboring Ho atom in the heterodimer.

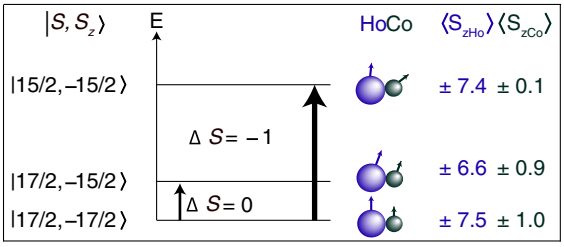

FIG. 4. Schematic of the magnetic sublevels involved in the SES process. The $\Delta S = -1$ transition (thick arrow) causes the high energy dI/dV steps and implies a large change in $S_{z,\mathrm{Co}}$ and, therefore, has a large signal. The low energy steps are due to a $\Delta S = 0$ transition where $S_{z,\mathrm{Co}}$ changes only slightly (thin arrow).

In conclusion, we detected spin excitations of individual exchange-coupled RE-TM heterodimers. The spectroscopic cross section mostly results from the out-of-plane projected spin variations in the 3d element. The possibility of detecting inelastic transitions of magnetic origin in RE based nanostructures allows unprecedented access to their magnetic level diagram, as well as their internal magnetic coupling.

We acknowledge funding from the Swiss National Science Foundation (SNSF) through Grants No. 200020–No. 157081 (A. S.), No. PP00P2_176866 and No. PZ00P2_167965 (F. D. N.), No. PZ00P2–No. 142474 (C. W.), and No. IZ73Z0–No. 152406 (S. S.). S. S., Z. S. P., and Ž. Š. acknowledge funding from the Serbian Ministry of Education and Science (Grant No. OI–171033). The DFT calculations were performed at UK (Archer) and Swedish (Beskow) supercomputing facilities, available through Grant No. PRACE DECI–13.

[1] P. C. M. Gubbens and K. H. J. Buschow, J. Appl. Phys. **44**, 3739 (1973).
[2] I. A. Campbell, J. Phys. F **2**, L47 (1972).
[3] L. T. Baczewski, D. Givord, J. M. Alameda, B. Dieny, J. Nozieres, J. P. Rebouillat, and J. J. Prejean, Acta Phys. Pol. A **83**, 629 (1993).
[4] A. Mishra, W. Wernsdorfer, K. A. Abboud, and G. Christou, J. Am. Chem. Soc. **126**, 15648 (2004).
[5] J. Dreiser, K. S. Pedersen, T. Birk, M. Schau-Magnussen, C. Piamonteze, S. Rusponi, T. Weyhermüller, H. Brune, F. Nolting, and J. Bendix, J. Phys. Chem. A **116**, 7842 (2012).
[6] R. Westerström, J. Dreiser, C. Piamonteze, M. Muntwiler, S. Weyeneth, H. Brune, S. Rusponi, F. Nolting, A. Popov, S. Yang, L. Dunsch, and T. Greber, J. Am. Chem. Soc. **134**, 9840 (2012).
[7] V. Vieru, L. Ungur, and L. F. Chibotaru, J. Phys. Chem. Lett. **4**, 3565 (2013).
[8] R. Westerström, A.-C. Uldry, R. Stania, J. Dreiser, C. Piamonteze, M. Muntwiler, F. Matsui, S. Rusponi,

H. Brune, S. Yang, A. Popov, B. Büchner, B. Delley, and T. Greber, Phys. Rev. Lett. **114**, 087201 (2015).
[9] A. J. Heinrich, J. A. Gupta, C. P. Lutz, and D. M. Eigler, Science **306**, 466 (2004).
[10] D. Coffey, J. L. Diez-Ferrer, D. Serrate, M. Ciria, C. d. l. Fuente, and J. I. Arnaudas, Sci. Rep. **5**, 13709 (2015).
[11] M. Steinbrecher, A. Sonntag, M. dos Santos Dias, M. Bouhassoune, S. Lounis, J. Wiebe, R. Wiesendanger, and A. A. Khajetoorians, Nat. Commun. **7**, 10454 (2016).
[12] M. Bode, M. Getzlaff, and R. Wiesendanger, Phys. Rev. Lett. **81**, 4256 (1998).
[13] T. Schuh, T. Miyamachi, S. Gerstl, M. Geilhufe, M. Hoffmann, S. Ostanin, W. Hergert, A. Ernst, and W. Wulfhekel, Nano Lett. **12**, 4805 (2012).
[14] T. Miyamachi, T. Schuh, T. Markl, C. Bresch, T. Balashov, A. Stohr, C. Karlewski, S. Andre, M. Marthaler, M. Hoffmann, M. Geilhufe, S. Ostanin, W. Hergert, I. Mertig, G. Schon, A. Ernst, and W. Wulfhekel, Nature (London) **503**, 242 (2013).
[15] T. Balashov, T. Miyamachi, T. Schuh, T. Märkl, C. Bresch, and W. Wulfhekel, Surf. Sci. **630**, 331 (2014).
[16] F. Donati, A. Singha, S. Stepanow, C. Wäckerlin, J. Dreiser, P. Gambardella, S. Rusponi, and H. Brune, Phys. Rev. Lett. **113**, 237201 (2014).
[17] I. G. Rau, S. Baumann, S. Rusponi, F. Donati, S. Stepanow, L. Gragnaniello, J. Dreiser, C. Piamonteze, F. Nolting, S. Gangopadhyay, O. R. Albertini, R. M. Macfarlane, C. P. Lutz, B. A. Jones, P. Gambardella, A. J. Heinrich, and H. Brune, Science **344**, 988 (2014).
[18] See Supplemental Material at http://link.aps.org/supplemental/10.1103/PhysRevLett.121.257202 for details on MgO preparation, DFT calculations, and the spin-Hamiltonian model, which also includes Refs. [19–32].
[19] J. Pal, M. Smerieri, E. Celasco, L. Savio, L. Vattuone, and M. Rocca, Phys. Rev. Lett. **112**, 126102 (2014).
[20] B. Bryant, A. Spinelli, J. J. T. Wagenaar, M. Gerrits, and A. F. Otte, Phys. Rev. Lett. **111**, 127203 (2013).
[21] D. Gatteschi, R. Sessoli, and J. Villain, in *Molecular Nanomagnets* (Oxford Scholarship Online, Oxford, 2006).
[22] W. Wernsdorfer and R. Sessoli, Science **284**, 133 (1999).
[23] K. Blum, *Density Matrix Theory and Applications* (Springer-Verlag, Berlin, Heidelberg, 2012).
[24] A. Singha, Ph.D. thesis, Ecole Polytechnique Federal de Lausanne, 2017.
[25] T. Ozaki, Phys. Rev. B **67**, 155108 (2003).
[26] I. Morrison, D. M. Bylander, and L. Kleinman, Phys. Rev. B **47**, 6728 (1993).
[27] OpenMX, open source package for material explorer, http://www.openmx-square.org/.
[28] J. P. Perdew, K. Burke, and M. Ernzerhof, Phys. Rev. Lett. **77**, 3865 (1996).
[29] V. I. Anisimov, J. Zaanen, and O. K. Andersen, Phys. Rev. B **44**, 943 (1991).
[30] H. J. Monkhorst and J. D. Pack, Phys. Rev. B **13**, 5188 (1976).
[31] D. C. Liu and J. Nocedal, Math. Program. **45**, 503 (1989).
[32] N. Ishikawa, M. Sugita, T. Okubo, N. Tanaka, T. Iino, and Y. Kaizu, Inorg. Chem. **42**, 2440 (2003).
[33] F. Donati, S. Rusponi, S. Stepanow, C. Wäckerlin, A. Singha, L. Persichetti, R. Baltic, K. Diller, F. Patthey, E. Fernandes, J. Dreiser, Ž. Šljivančanin, K. Kummer, C. Nistor, P. Gambardella, and H. Brune, Science **352**, 318 (2016).
[34] F. D. Natterer, K. Yang, W. Paul, P. Willke, T. Choi, T. Greber, A. J. Heinrich, and C. P. Lutz, Nature (London) **543**, 226 (2017).
[35] F. D. Natterer, F. Donati, F. Patthey, and H. Brune, Phys. Rev. Lett. **121**, 027201 (2018).
[36] C. Wäckerlin, F. Donati, A. Singha, R. Baltic, S. Rusponi, K. Diller, F. Patthey, M. Pivetta, Y. Lan, S. Klyatskaya, M. Ruben, H. Brune, and J. Dreiser, Adv. Mater. **28**, 5195 (2016).
[37] L. Claude, Ph. D. thesis, École Polytechnique Fédéral de Lausanne, 2005.
[38] E. Fernandes, F. Donati, F. Patthey, S. Stavrić, Ž. Šljivančanin, and H. Brune, Phys. Rev. B **96**, 045419 (2017).
[39] S. Baumann, F. Donati, S. Stepanow, S. Rusponi, W. Paul, S. Gangopadhyay, I. G. Rau, G. E. Pacchioni, L. Gragnaniello, M. Pivetta, J. Dreiser, C. Piamonteze, C. P. Lutz, R. M. Macfarlane, B. A. Jones, P. Gambardella, A. J. Heinrich, and H. Brune, Phys. Rev. Lett. **115**, 237202 (2015).
[40] W. Paul, K. Yang, S. Baumann, N. Romming, T. Choi, C. P. Lutz, and A. J. Heinrich, Nat. Phys. **13**, 403 (2017).
[41] T. Schuh, T. Balashov, T. Miyamachi, A. F. Takács, S. Suga, and W. Wulfhekel, J. Appl. Phys. **107**, 09E156 (2010).
[42] S. Baumann, Ph. D. thesis, University of Basel, 2015.
[43] S. Loth, K. von Bergmann, M. Ternes, A. F. Otte, C. P. Lutz, and A. J. Heinrich, Nat. Phys. **6**, 340 (2010).
[44] J. Dreiser, J. Phys. Condens. Matter **27**, 183203 (2015).
[45] C. F. Hirjibehedin, C.-Y. Lin, A. F. Otte, M. Ternes, C. P. Lutz, B. A. Jones, and A. J. Heinrich, Science **317**, 1199 (2007).
[46] A. F. Otte, M. Ternes, K. von Bergmann, S. Loth, H. Brune, C. P. Lutz, C. F. Hirjibehedin, and A. J. Heinrich, Nat. Phys. **4**, 847 (2008).
[47] Y. Janssen, Ph. D. thesis, Universiteit van Amsterdam, 2003.
[48] P. Gambardella, S. Rusponi, M. Veronese, S. S. Dhesi, C. Grazioli, A. Dallmeyer, I. Cabria, R. Zeller, P. H. Dederichs, K. Kern, C. Carbone, and H. Brune, Science **300**, 1130 (2003).
[49] F. Donati, L. Gragnaniello, A. Cavallin, F. D. Natterer, Q. Dubout, M. Pivetta, F. Patthey, J. Dreiser, C. Piamonteze, S. Rusponi, and H. Brune, Phys. Rev. Lett. **113**, 177201 (2014).